Research Article | Vol. 32, No. 15 / 15 Jul 2024 / Optics Express 25717
Optics EXPRESS

Measurements of cesium P_J-series quantum defect with the microwave spectroscopy

Rong Song,[1] Jingxu Bai,[1] Zhenhua Li,[1] Yuechun Jiao,[1,2,*] Jianming Zhao,[1,2,3] and Suotang Jia[1,2]

[1]State Key Laboratory of Quantum Optics and Quantum Optics Devices, Institute of Laser Spectroscopy, Shanxi University, Taiyuan 030006, China
[2]Collaborative Innovation Center of Extreme Optics, Shanxi University, Taiyuan 030006, China
[3]zhaojm@sxu.edu.cn
[*]ycjiao@sxu.edu.cn

Abstract: High-precision microwave spectroscopy has been used to measure the transition frequency of $nS_{1/2} \rightarrow nP_J$ (n is the principle quantum number) and further the quantum defect of nP_J states in a standard cesium magneto-optical trap. A microwave field with 30-μs duration coupling the $nS_{1/2} \rightarrow nP_{1/2,3/2}$ transition yields a narrow linewidth microwave spectroscopy with the linewidth approaching the Fourier limit. After carefully compensating the stray electric and magnetic field and using the diluted atomic gas, we extract improved quantum defects of nP_J state, $\delta_0(nP_{1/2}) = 3.59159091(19)$, $\delta_2(nP_{1/2}) = 0.36092(35)$ and $\delta_0(nP_{3/2}) = 3.55907153(25)$, $\delta_2(nP_{3/2}) = 0.37344(47)$.

1. Introduction

Precise measurement of atomic transition frequency and atomic level is significant for applications of atomic clocks [1–3] and quantum information science [4,5] and microwave field metrology [6] and Rydberg molecules [7,8]. Due to the interaction between the ionic core and the valence electron, the energy level of alkali-metal for $l \leq 3$ state (l is the angular momentum quantum number) is depressed below the expected hydrogenic level, which is known as the quantum defect. The accurate quantum defect values are very important not only for understanding of the atomic structure but also helpful for determination of the Rydberg wave function and calculations of Stark effect [9] and Rydberg molecular potential. Cold atomic sample, often used in these measurements, combines the narrow linewidth microwave spectroscopy allowing one to obtain precise Rydberg transition frequency, and further the Rydberg level with the Rydberg formula.

Measurements of the quantum defects have been done in Alkali atoms [10–23]. For cesium atom, Rydberg energy levels have been determined using classical methods, such as grating and interference spectroscopy [24], high-resolution Fourier spectroscopy [25], Doppler-free laser spectroscopy [26–29], resonance-enhanced Doppler-free multiphoton spectra [30,31], and so on. Weber et al [12] measured Rydberg energies of cesium nS, nP, nD, nF and nG states and obtained the quantum defect values with a spectral accuracy of 5 MHz, which are the most widely used today. The quantum defects of S, P, D and F levels are measured by the high-resolution double-resonance spectroscopy with an accuracy of about 1 MHz [32]. The transition frequencies and improved quantum defect values of $nS_{1/2}$, $nP_{1/2,3/2}$, $nD_{5/2}$ are determined by one-photon UV spectroscopy in ultracold Cs atoms using a narrow-band laser excitation [33].

In this work, we present measurements of quantum defect of cesium Rydberg nP_J states ($n = 41 - 55$) by employing the precise microwave spectroscopy. Cesium atoms are laser-cooled and trapped in a magneto-optical trap (MOT). $nS_{1/2}$ Rydberg states are populated with a two-step excitation scheme and coupled by a microwave field between $nS_{1/2}$ and nP_J states, yielding the microwave spectroscopy. To decrease the effect of the stray electric and magnetic field, we carefully compensate the stray electric and magnetic fields to below 2 mV/cm and 5 mG in the

#528290 https://doi.org/10.1364/OE.528290
Journal © 2024 Received 24 Apr 2024; revised 11 Jun 2024; accepted 18 Jun 2024; published 2 Jul 2024

Optics EXPRESS

MOT center with Stark and Zeeman effect, respectively. The narrowest linewidth of microwave spectroscopy is 36 kHz, approaching the Fourier-transform limit. The weighted center frequency of $n\mathrm{S}_{1/2} \rightarrow n\mathrm{P}_\mathrm{J}$ and the quantum defect of $n\mathrm{P}_\mathrm{J}$ state are extracted. Our results show a good agreement with the literature values.

2. Experimental setup

The schematic of our experiment is shown in Fig. 1(a). Cesium atoms are laser-cooled and trapped in a metal chamber with the vacuum pressure of 1×10^{-7} Pa. The MOT temperature and peak density are $\sim 100\ \mu$K and $\sim 10^{10}$ cm^{-3}, measured with an absorption imaging method [34]. The details of experiments see our previous work [35,36]. After switching off the MOT beam, we apply a two-step excitation pulse with 500 ns duration to populate the $nS_{1/2}$ Rydberg state, see Fig. 1(b). Two lasers are locked to an ultrastable Fabry−Pérot cavity with the finesse of 15000 employing the Pound-Drever-Hall (PDH) method. The laser linewidth after locking is less than 50 kHz. The effective Rabi frequency is $\Omega = \Omega_{852}\Omega_{510}/2\delta = 2\pi \times 20$ kHz. The small Rabi frequency and short pulse duration of excitation laser are used for decreasing Rydberg populations and further the interaction induced shift. After the laser pulse, we apply a 30-μs duration microwave (Analog Signal Generator N5183B) pulse for coupling the Rydberg transition $n\mathrm{S}_{1/2} \rightarrow n\mathrm{P}_\mathrm{J}$, forming the narrow linewidth microwave spectroscopy. Finally, we apply a 3-μs ramped electric field to state selective field ionize Rydberg atoms, a detailed time sequence is shown in Fig. 1(c). Time-resolved ion signal is collected with a microchannel plate (MCP) detector and recorded with a boxcar integrator (SRS-250) and processed on a computer. Furthermore, three pairs of grids and Helmholtz coils are placed to compensate stray electric and magnetic fields with Stark and Zeeman effects. The stray electric and magnetic fields are less than 2 mV/cm and 5 mG after compensation, respectively. The detailed compensation procedure see our previous work [35].

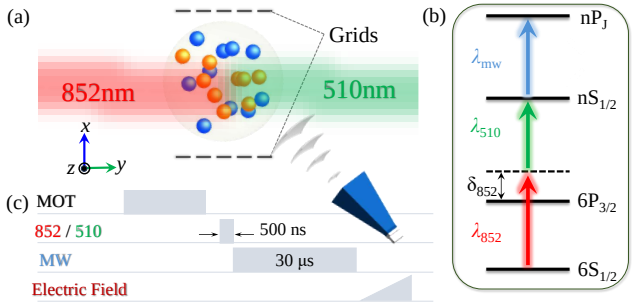

Fig. 1. (a) Experimental setup. Two excitation beams, 852-nm and 510-nm lasers, are counter-propagated through the MOT center to populate the $n\mathrm{S}_{1/2}$ Rydberg state. Three pairs of grids and Helmholtz coils are used to compensate stray electric and magnetic fields, respectively. Here we only show one pair of grids in x direction. A microwave field, emitted with an antenna, couples the transition of $n\mathrm{S}_{1/2} \rightarrow n\mathrm{P}_\mathrm{J}$. The laser excited $n\mathrm{S}_{1/2}$ state and microwave coupled $n\mathrm{P}_\mathrm{J}$ Rydberg atom are detected by the state selective field ionization technique. (b) Level diagram of the excitation scheme. The $n\mathrm{S}_{1/2}$ states are excited with the two-step resonant excitation with the first-step laser detuned $\delta_{852}/2\pi = +330$ MHz to the intermediate $6\mathrm{P}_{3/2}$ state. The first-step laser (λ_{852}) drives the ground-state transition and the second-step laser (λ_{510}) couples Rydberg transition. A Microwave field λ_{mw} couples the Rydberg transition $n\mathrm{S}_{1/2} \rightarrow n\mathrm{P}_{1/2,3/2}$. (c) Timing sequence of experiments. After switching off the MOT beam, we apply a 500-ns laser pulse to populate the $n\mathrm{S}_{1/2}$ launch state and then a 30-μs microwave pulse to couple the $n\mathrm{S}_{1/2} \rightarrow n\mathrm{P}_\mathrm{J}$ transition. Finally, a ramped electric field is applied for state selective field ionization of Rydberg atoms.

Optics EXPRESS

Figure 1(b) displays the level diagram, the first-step laser excites the $6S_{1/2}, F = 4 \rightarrow 6P_{3/2}, F' = 5$ transition, whereas the second-step laser couples $6P_{3/2}, F' = 5 \rightarrow nS_{1/2}$ transition. To reduce photon scattering and light radiation pressure, the first-step excitation is blue-detuned from the intermediate $6P_{3/2}, F' = 5$ state by $\delta_{852}/2\pi = 330$ MHz.

3. Microwave spectroscopy

In the experiment, we lock the laser frequency to resonantly excite $nS_{1/2}$ state ($n = 41-55$) and the microwave field couples the $nS_{1/2} \rightarrow nP_J$ transition. In Fig. 2, we display measured microwave spectra of the transition $51S_{1/2}$ to $51P_{1/2}$ (a) and $51P_{3/2}$ (b). It is found that the microwave spectrum in Fig. 2(a) for $51P_{1/2}$ state clearly shows two peaks, which is attributed to the hyperfine transitions of $51S_{1/2}, F = 4$ to $51P_{1/2}, F' = 3$ and $F' = 4$, respectively. The multiple Lorentzian fitting (solid line) yields respective hyperfine transition frequencies of 28.67847831(78) GHz and 28.67862139(63) GHz with the statistical uncertainty less than 1 kHz. We further obtain the weighted center frequency of $51P_{1/2}$, 28.67855880(100) GHz. Figure 2(b) displays the microwave spectrum of $51S_{1/2}, F = 4 \rightarrow 51P_{3/2}$ transition. Because the hyperfine interval of the $51P_{3/2}$ state are too small to be distinguished, the spectrum only shows one broadened resonance peak. The Lorentzian fitting (solid line) yields the transition frequency of 30.6842610(23) GHz with a statistical uncertainty of approximately 2 kHz. The residuals analysis demonstrates that the single Lorentzian fitting is a good fit for attaining the transition frequency of $nS_{1/2} \rightarrow nP_{3/2}$. Due to indistinguishable hyperfine structure and broadened linewidth, the statistical error for $51P_{3/2}$ state is two times larger than for $51P_{1/2}$ state. The extracted transition frequencies are listed in Table 2.

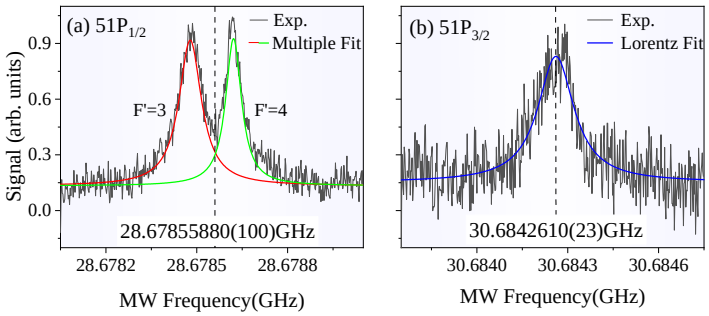

Fig. 2. Measured microwave spectra of Rydberg transition $51S_{1/2}, F = 4 \rightarrow 51P_{1/2}, F'$ (a) and $51P_{3/2}$ state (b). Black lines show the detected nP Rydberg transition probability signal, which are the average of five independent measurements. The solid lines are Lorentzian fittings. For $51P_{1/2}$ state in (a), the microwave spectrum displays two peaks coming from the hyperfine structure of F'=3 and F'=4. The vertical dashed line marks the weighted center frequency of $51S_{1/2} \rightarrow 51P_{1/2}$ transition. For $51P_{3/2}$ in (b), spectrum displays one peak with broadened linewidth, a Lorentzian fitting yields the central frequency of $51S_{1/2} \rightarrow 51P_{3/2}$ transition, marked with a vertical dashed line.

4. Systematic uncertainty

For precision spectroscopic measurements, an analysis of the uncertainty caused by systematic effects is an important part. In this section, we will analyze our systematic uncertainties due to the stray electric and magnetic fields, as well as Rydberg-atom interactions. The detailed analysis of the uncertainty is similar to our previous work [36], here we simply discuss the systematic uncertainty arising from the stray electric and magnetic fields and Rydberg-atom interactions.

Optics EXPRESS

In this work, we investigate the microwave spectroscopy of $n\mathrm{S}_{1/2}, \mathrm{F} = 4 \rightarrow n\mathrm{P}_\mathrm{J}$ transition. Firstly, we discuss Stark effect induced level shifts. DC Stark shifts have been reduced by compensating the stray electric field via the Stark map of microwave spectroscopy. In Fig. 3(a), we present the contour plot of Stark map for the electric field being applied in the x direction E_x, (setting E_y and E_z zero or compensated value), from which we can extract the compensating field of x-direction. We then set E_x to be the compensating field and use the same procedure to obtain the compensating field in y- and z-direction. By comparing the measurement and calculation of the microwave spectrum, we can extract the stray electric field after compensation, which is less than 2 mV/cm. Figure 3(b) displays the measured Stark shift for $E_i \leq 2$ mV/cm ($i = x, y$ and z). We use the standard error of the mean (SEM) of the data points in Fig. 3(b) to estimate the systematic shift due to the electric field, the attained SEM is 0.8 kHz. During the experiments, we have verified the DC electric-field compensation every day throughout the data taking.

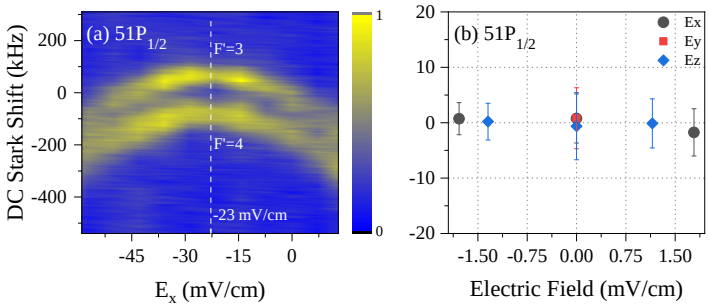

Fig. 3. (a) Contour plot of Stark spectra of microwave field coupling the transition $51\mathrm{S}_{1/2} \rightarrow 51\mathrm{P}_{1/2}$ for the electric field applied in x-direction and setting $E_y = 0$ and $E_z = 0$. The spectroscopy shows symmetrical Stark shift of hyperfine structure of $51\mathrm{P}_{1/2}, \mathrm{F}' = 3, 4$. The zero field represents the potential we applied to the electrode is zero. A vertical white dashed line indicates compensation value of 23 mV/cm in x direction, where there is no Stark shift. (b) Measured DC Stark shifts of weighted center frequency for $51\mathrm{P}_{1/2}$ state as a function of the electric fields in three directions. The error bars are the SEM of five independent measurements. The SEM of seven data is taken to estimate the systematic shift caused by the electric field.

We secondly discuss the level shift induced by the magnetic field. For analyzing the systematic uncertainties due to the magnetic field, we investigate the Zeeman effect by applying the current in the Helmholtz coils in three directions. The Zeeman splitting spectra and magnetic-field compensation process are described in [35–37]. The residual magnetic field is estimated to be ≤ 5 mG after compensating. For the weak field range (≤ 40 mG), calculations of Zeeman spectra [37] demonstrate that the hyperfine splitting of $51\mathrm{P}_{1/2}$ is larger than the Zeeman shift, the spectra are in the Zeeman effect regime. The spectrum shows the linear Zeeman splitting and symmetric line broadening in linear Zeeman regime. We have eliminated the Zeeman splittings and line broadening by varying magnetic field. To analyze the uncertainty from magnetic field, we make the measurements of the microwave spectroscopy like in Fig. 2(a) for different magnetic field of $\lesssim 5$ mG and obtain the averaged center frequency of $51\mathrm{S}_{1/2} \rightarrow 51\mathrm{P}_{1/2}$. The SEM analysis yields $\Delta\nu_{P_{1/2}} = 0.5$ kHz due to magnetic field.

We thirdly consider the shift due to the interaction between Rydberg atoms. Rydberg energy level can be shifted due to the dipole-dipole interaction, scaling as C_3/R^3, and van-der-Waals interaction, scaling as C_6/R^6, between Rydberg atoms. To decrease the systematic uncertainty due to the Rydberg interaction, we increase the beam waist of excitation laser and decrease the laser power to decrease Rydberg excitation probability. The density of estimated $n\mathrm{S}_{1/2}$ Rydberg atoms is $\leq 3 \times 10^6$ cm^{-3}, corresponding atomic separation $R \approx 40$ μm. The calculated C_6 is

Optics EXPRESS

14 GHzμm^6 for $51S_{1/2}$ state and -2 GHzμm^6 for $51P_{1/2}$ state, which yields level shifts due to Van der Waals interaction of tens of Hz and are negligible. For $51S_{1/2} - 51P_{1/2}$ pair states, the calculated C_3 is 0.74 GHzμm^3, leading to line shifts to be 7.6 kHz. It is noted that the dipolar interaction potentials are distributed symmetrically about the asymptotic energies, which means that the attractive potentials are same as the repulsive potentials. Therefore the main effect of the dipolar interactions is a line broadening. We make multiple measurements of microwave spectroscopy for $51S_{1/2} \rightarrow 51P_{1/2}$ transition by changing the Rydberg density via decreasing the 510 nm laser power, SEM analysis of frequency shift yields uncertainty is 0.6 kHz.

We next discuss the systematic uncertainty arising from AC Stark effect. The microwave intensity at the MOT center is varied by changing the synthesizer output power. We measure a series of the microwave spectra of $51S_{1/2} \rightarrow 51P_{1/2}$ transition for different microwave powers and extract the averaged center frequency. We found that when the synthesizer output is less than -70 dBm, corresponding microwave field in MOT center less than 0.0024V/m (field calibration see Ref. [36]), and AC Stark shift estimated to be a few Hz, that has a negligible effect. Therefore we do the multiple measurements at weak microwave field to decrease the systematic uncertainty, and the systematic uncertainty due to AC Stark effect is included in statistics uncertainty.

Finally we consider the other facts that may lead the systematic uncertainty. For example, the systematic shift due to signal-generator frequency uncertainty is less than 10 Hz, that is negligible. To summarize the systematic shift discussed above, we list these systematic uncertainties in Table 1. We can see that the all systematic uncertainty in this work is less than 2 kHz.

Table 1. Summary of systematic uncertainty in kHz.

Source	$\Delta\nu_{P_{1/2}}$ (kHz)
Interactions	0.6
Electric Field	0.8
Magnetic Field	0.5
Δ_{total}	1.1

5. Results and discussions

The transition frequency of $nS_{1/2} \rightarrow nP_J$ can be expressed by

$$\upsilon_{nS,nP_J} = R_{Cs}c\{[n - \delta_S(n)]^{-2} - [n - \delta_{P_J}(n)]^{-2}\}, \tag{1}$$

where R_{Cs}=10973686.274 m^{-1} is the Rydberg constant of cesium [38], c=2.99792458 $\times$ 10^8 m/s is the speed of light, $\delta_S(n)$ and $\delta_{P_J}(n)$ are the quantum defects of the initial and final states. From measured transition frequency and the known quantum defect value of the cesium $nS_{1/2}$ state [33], we can obtain the quantum defect of nP_J state using Eq. (1). We have performed a series of microwave-spectroscopy measurements of $nS_{1/2} \rightarrow nP_J$ transition, like Fig. 2, for $n = 41 - 55$ range. The extracted transition frequencies and their quantum defects are listed in Table 2. It is noted that for $n \leq 44$, the hyperfine structure of $nP_{3/2}$ microwave spectrum also can be distinguished, where multiple Lorentzian fitting is employed to extract the hyperfine transition frequency and further the weighted center frequency.

We next analyze the uncertainty of measured quantum defect. We rewrite the Eq. (1) as

$$\delta_{P_J}(n) = n - \frac{1}{\sqrt{[n - \delta_S(n)]^{-2} - \frac{\upsilon}{R_{Cs}c}}} = n - \frac{1}{\sqrt{\alpha}}, \tag{2}$$

Optics EXPRESS

Table 2. Measured transition frequencies (GHz) of $n\mathrm{S}_{1/2} \rightarrow n\mathrm{P_J}$ and corresponding quantum defects of $n\mathrm{P_J}$ state.

	Transition frequency (GHz)		$\delta_{\mathrm{P_J}}$	
n	$\mathrm{P}_{1/2}$	$\mathrm{P}_{3/2}$	$\mathrm{P}_{1/2}$	$\mathrm{P}_{3/2}$
41	58.599 448 74(097)	62.680 459 3(23)	3.591 848 91(57)	3.559 338 00(54)
42	54.114 687 70(106)	57.885 336 7(16)	3.591 835 63(55)	3.559 324 30(53)
43	50.076 137 11(097)	53.567 110 2(38)	3.591 823 32(54)	3.559 311 63(52)
44	46.429 655 30(108)	49.667 938 1(24)	3.591 811 88(53)	3.559 299 88(51)
48	34.926 240 99(097)	37.366 288 6(13)	3.591 773 75(49)	3.559 260 37(48)
49	32.658 098 59(107)	34.940 532 0(09)	3.591 765 97(49)	3.559 252 38(47)
51	28.678 558 80(100)	30.684 261 0(23)	3.591 751 36(47)	3.559 237 27(46)
53	25.320 174 29(188)	27.092 127 4(39)	3.591 738 75(47)	3.559 224 31(45)
55	22.466 341 76(221)	24.039 501 2(12)	3.591 727 65(46)	3.559 212 91(44)

where $\alpha = [n - \delta_{\mathrm{S}}(n)]^{-2} - \frac{\upsilon}{R_{Cs}c}$. Then the uncertainties of the measured quantum defects read [35]

$$\Delta\delta_{\mathrm{P_J}}(n) = \left(\frac{1}{2}\alpha^{-\frac{3}{2}}\right)\left\{\left(\frac{\upsilon}{R_{Cs}c}\right)^2\left[\left(\frac{\Delta\upsilon}{\upsilon}\right)^2 + \left(\frac{\Delta R_{Cs}}{R_{Cs}}\right)^2\right] + \left[2[n-\delta_{\mathrm{S}}(n)]^{-3}\Delta(n-\delta_{\mathrm{S}}(n))\right]^2\right\}^{\frac{1}{2}}. \quad (3)$$

From Eq. (3), the uncertainty of measured quantum defect includes, i) $\frac{\Delta R_{Cs}}{R_{Cs}} = 1.9 \times 10^{-12}$, the uncertainty of Rydberg constant has a negligible effect. ii) the frequency uncertainties of our measurements, $\frac{\Delta\upsilon}{\upsilon} = \frac{\sqrt{\Delta\upsilon_{stat}^2 + \Delta_{total}^2}}{\upsilon}$ is less than 1×10^{-7}, here the $\Delta\upsilon_{\mathrm{stat}}$ is the statistics uncertainty and Δ_{total} is the systematic uncertainty from Table 1. iii) The uncertainties $\Delta(n - \delta_{\mathrm{S}}(n))$ of the quantum defects of the $n\mathrm{S}_{1/2}$ states that come from [33]. Using Eq. (3), we attain the uncertainty of our measured quantum defects of $n\mathrm{P_J}$ states, which are listed in the Table 2. We found that the uncertainties of quantum defect for $n\mathrm{P_J}$ states are the same as that for the launch $n\mathrm{S}_{1/2}$ state. Therefore the uncertainty of launch $n\mathrm{S}_{1/2}$ state is the main source of our measurements.

From the Table 2, it is found that the quantum defects $\delta_{\mathrm{P_J}}$ show minor decrease with quantum number n. Using the extended Rydberg-Ritz formula [17], quantum defect δ_{nlJ} is usually written as,

$$\delta_{\mathrm{nlJ}} = \delta_0 + \frac{\delta_2}{(n-\delta_0)^2} + \frac{\delta_4}{(n-\delta_0)^4} + \cdots, \quad (4)$$

where the δ_i(i=0,2,4) are constants, and δ_0 is leading term. The quantum defect mainly depends on l and slightly on n and J. When n>20, we usually consider the first two factors, δ_0 and δ_2, in Eq. (4).

In order to obtain quantum defect parameters $\delta_i(\mathrm{P_J})$, we plot the measured quantum defects $\delta_{\mathrm{P_J}}$ in Table 2 as a function of $(n-\delta_{\mathrm{P_J}})^{-2} = n^{*-2}$ for J = 1/2 in Fig. 4(a) and J = 3/2 in Fig. 4(b). Here the $\delta_{\mathrm{P_J}}$ used in the evaluation of n^{*-2} is from Ref. [33]. The solid lines are fittings with Eq. (4) yielding $\delta_0(\mathrm{P}_{1/2}) = 3.59159091(19)$, $\delta_2(\mathrm{P}_{1/2}) = 0.36092(35)$ and $\delta_0(\mathrm{P}_{3/2}) = 3.55907153(25)$, $\delta_2(\mathrm{P}_{3/2}) = 0.37344(47)$, respectively. The δ_0 and δ_2 are listed in Table 3.

To compare with the previous works, in the Table 3, we also list the quantum defects of $\mathrm{P_J}$ state of previous work [12,32,33]. In [12], the quantum defect is obtained by resonant two-photon spectroscopy with the spectral accuracy of 5 MHz. In [33], the transition frequencies are determined by one-photon UV spectroscopy in ultracold cesium atoms using a narrow-band laser system referenced to a frequency comb, with the spectral linewidth of 1 MHz. Whereas the work [32] attained the quantum defect by the high-resolution double-resonance spectroscopy

Optics EXPRESS

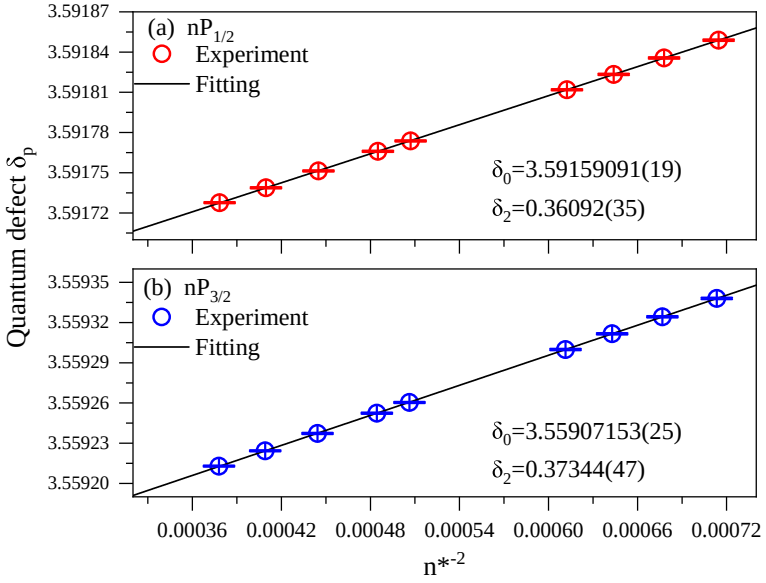

Fig. 4. Measurements of quantum defects $\delta_{P(n)}$ as a function of n^{*-2} for $n\mathrm{P}_{1/2}$ (a) and $n\mathrm{P}_{3/2}$ (b). The circles display our measurements taken from Table 2. The solid lines are the fittings with Eq. (4).

Table 3. Comparison of the quantum defect δ_0 and δ_2 for $n\mathrm{P_J}$ in this and previous works [12,32,33].

	$n\mathrm{P}_{1/2}$		$n\mathrm{P}_{3/2}$	
	δ_0	δ_2	δ_0	δ_2
this work (n=41-55)	3.59159091(19)	0.36092(35)	3.55907153(25)	0.37344(47)
[33] (n=27-74)	3.5915871(3)	0.36273(16)	3.5590676(3)	0.37469(14)
[32] (n=23-45)	3.591556(30)	0.3714(40)	3.559058(30)	0.374(4)
[12] (n= 6-80)	3.59158950(58)	0.360926		

with an accuracy of about 1 MHz. In our work, we obtain the quantum defect of $n\mathrm{P_J}$ state by using the microwave spectroscopy with the spectral accuracy of tens of kHz, and the statistics uncertainty less than 2 kHz. During the experimental progress, we carefully compensate the electric and magnetic field by Stark and Zeeman effect, further we use diluted atomic gas to reduce the interaction induced shift, the total systematic uncertainty is estimated to be 1.1 kHz. The measured quantum defects of δ_0 and δ_2 for $\mathrm{P}_{1/2}$ are agreement with the previous work [12]. For the quantum defect of $\mathrm{P}_{3/2}$ state, our measurement shows agreement with that in [32,33] and more precise.

6. Conclusions

We have investigated microwave spectroscopy within magneto-optically trapped cesium atoms, where the microwave field couples the $n\mathrm{S}_{1/2} - n\mathrm{P_J}$ transition. By reducing the Rydberg interaction induced shift, and Stark and Zeeman shift, we have measured the microwave transition frequency with uncertainty less than 2 kHz and obtained an improved quantum defect of cesium $n\mathrm{P}_{1/2,3/2}$ Rydberg state. Measured quantum defects δ_0 and δ_2 are agreement with the previous works [12,32,33]. This work on the quantum defect measurement of cesium $n\mathrm{P}_{1/2,3/2}$ Rydberg state is significant not only for calculation of the Stark effect, but also helpful for further determination of the Rydberg wave function and adiabatic energy potential curve of Rydberg molecules. The

Optics EXPRESS

accurate measurement of the Rydberg level and quantum defect are also significant for the Rydberg-atom based microwave sensor and the field metrology.

Funding. National Natural Science Foundation of China (12120101004, 12241408, 62175136, U2341211); Fundamental Research Program of Shanxi Province (202303021224007); Changjiang Scholars and Innovative Research Team in Universities of the Ministry of Education of China (IRT 17R70); 1331 project of Shanxi Province.

Disclosures. The authors declare no conflicts of interest.

Data availability. Data underlying the results presented in this paper are not publicly available at this time but may be obtained from the authors upon reasonable request.

References

1. B. J. Bloom, T. L. Nicholson, J. R. Williams, *et al.*, "An optical lattice clock with accuracy and stability at the 10^{-18} level," Nature **506**(7486), 71–75 (2014).
2. K. W. Martin, G. Phelps, N. D. Lemke, *et al.*, "Compact optical atomic clock based on a two-photon transition in rubidium," Phys. Rev. Appl. **9**(1), 014019 (2018).
3. C. J. Kennedy, E. Oelker, J. M. Robinson, *et al.*, "Precision metrology meets cosmology: improved constraints on ultralight dark matter from atom-cavity frequency comparisons," Phys. Rev. Lett. **125**(20), 201302 (2020).
4. A. Gaëtan, Y. Miroshnychenko, T. Wilk, *et al.*, "Observation of collective excitation of two individual atoms in the Rydberg blockade regime," Nat. Phys. **5**(2), 115–118 (2009).
5. E. Urban, T. A. Johnson, T. Henage, *et al.*, "Observation of Rydberg blockade between two atoms," Nat. Phys. **5**(2), 110–114 (2009).
6. J. A. Sedlacek, A. Schwettmann, H. Kübler, *et al.*, "Microwave electrometry with Rydberg atoms in a vapour cell using bright atomic resonances," Nat. Phys. **8**(11), 819–824 (2012).
7. V. Bendkowsky, B. Butscher, J. Nipper, *et al.*, "Observation of ultralong-range Rydberg molecules," Nature **458**(7241), 1005–1008 (2009).
8. K. R. Overstreet, A. Schwettmann, J. Tallant, *et al.*, "Observation of electric-field-induced Cs Rydberg atom macrodimers," Nat. Phys. **5**(8), 581–585 (2009).
9. G. D. Stevens, C.-H. Iu, T. Bergeman, *et al.*, "Precision measurements on lithium atoms in an electric field compared with *R* -matrix and other Stark theories," Phys. Rev. A **53**(3), 1349–1366 (1996).
10. J. R. McNally, J. P. Molnar, W. J. Hitchcock, *et al.*, "High Members of the Principal Series in Caesium," J. Opt. Soc. Am. **39**(1), 57–58 (1949).
11. H. R. Kratz, "The Principal Series of Potassium, Rubidium, and Cesium in Absorption," Phys. Rev. **75**(12), 1844–1850 (1949).
12. K.-H. Weber and C. J. Sansonetti, "Accurate energies of *nS*, *nP*, *nD*, *nF*, and *nG* levels of neutral cesium," Phys. Rev. A **35**(11), 4650–4660 (1987).
13. W. Li, I. Mourachko, M. W. Noel, *et al.*, "Millimeter-wave spectroscopy of cold Rb Rydberg atoms in a magneto-optical trap: Quantum defects of the ns, np, and nd series," Phys. Rev. A **67**(5), 052502 (2003).
14. J. Han, Y. Jamil, D. V. L. Norum, *et al.*, "Rb nf quantum defects from millimeter-wave spectroscopy of cold ^{85}Rb Rydberg atoms," Phys. Rev. A **74**(5), 054502 (2006).
15. J. Lee, J. Nunkaew, and T. F. Gallagher, "Microwave spectroscopy of the cold rubidium $(n+1)d_{5/2} \rightarrow ng$ and nh transitions," Phys. Rev. A **94**(2), 022505 (2016).
16. R. Cardman and G. Raithel, "Hyperfine structure of $nP_{1/2}$ Rydberg states in ^{85}Rb," Phys. Rev. A **106**(5), 052810 (2022).
17. C.-J. Lorenzen and K. Niemax, "Quantum Defects of the $n^2P_{1/2,3/2}$ Levels in ^{39} K I and ^{85} Rb I," Phys. Scr. **27**(4), 300–305 (1983).
18. K. Moore, A. Duspayev, R. Cardman, *et al.*, "Measurement of the Rb g-series quantum defect using two-photon microwave spectroscopy," Phys. Rev. A **102**(6), 062817 (2020).
19. H. Lehec, A. Zuliani, W. Maineult, *et al.*, "Laser and microwave spectroscopy of even-parity Rydberg states of neutral ytterbium and multichannel-quantum-defect-theory analysis," Phys. Rev. A **98**(6), 062506 (2018).
20. L. R. Pendrill, D. Delande, and J. C. Gay, "Quantum defect and fine-structure measurements of P, D, F and G Rydberg states of atomic caesium," J. Phys. B: At. Mol. Phys. **12**(20), L603–L608 (1979).
21. R. R. Freeman and D. Kleppner, "Core polarization and quantum defects in high-angular-momentum states of alkali atoms," Phys. Rev. A **14**(5), 1614–1619 (1976).
22. K. Afrousheh, P. Bohlouli-Zanjani, J. A. Petrus, *et al.*, "Determination of the ^{85}Rb ng-series quantum defect by electric-field-induced resonant energy transfer between cold Rydberg atoms," Phys. Rev. A **74**(6), 062712 (2006).
23. S. B. S. , S. K. Barik, S. Chaudhuri, *et al.*, "Transition frequency measurement of highly excited Rydberg states of ^{87}Rb for a wide range of principal quantum numbers," Opt. Continuum **1**(5), 1176 (2022).
24. H. Kleiman, "Interferometric measurements of cesium i," J. Opt. Soc. Am. **52**(4), 441–447 (1962).
25. C. J. Sansonetti, K. L. Andrew, and J. Verges, "Polarization, penetration, and exchange effects in the hydrogenlike nf and ng terms of cesium," J. Opt. Soc. Am. **71**(4), 423–433 (1981).
26. C.-J. Lorenzen, K.-H. Weber, and K. Niemax, "Energies of the n^2s_{12} and $n^2d_{32,52}$ states of cs," Opt. Commun. **33**(3), 271–276 (1980).

Optics EXPRESS

27. C. J. Lorenzen and K. Niemax, "Non-monotonic variation of the quantum defect in Cs nD$_J$ term series," Z. Phys. A: At. Nucl. **311**(3), 249–250 (1983).
28. C. J. Lorenzen and K. Niemax, "Precise quantum defects of nS, nP and nD Levels in Cs I," Z. Phys. A: At. Nucl. **315**(2), 127–133 (1984).
29. M. S. O'Sullivan and B. P. Stoicheff, "Doppler-free two-photon absorption spectrum of cesium," Can. J. Phys. **61**(6), 940–948 (1983).
30. J. E. Bjorkholm and P. F. Liao, "Line shape and strength of two-photon absorption in an atomic vapor with a resonant or nearly resonant intermediate state," Phys. Rev. A **14**(2), 751–760 (1976).
31. P. F. Liao and J. E. Bjorkholm, "Measurement of the fine-structure splitting of the 4F state in atomic sodium using two-photon spectroscopy with a resonant intermediate state," Phys. Rev. Lett. **36**(26), 1543–1545 (1976).
32. P. Goy, J. M. Raimond, G. Vitrant, *et al.*, "Millimeter-wave spectroscopy in cesium Rydberg states: quantum defects, fine- and hyperfine-structure measurements," Phys. Rev. A **26**(5), 2733–2742 (1982).
33. J. Deiglmayr, H. Herburger, H. Saßmannshausen, *et al.*, "Precision measurement of the ionization energy of Cs *I*," Phys. Rev. A **93**(1), 013424 (2016).
34. C. J. Foot, *Atomic Physics* (Oxford University Press, 2004).
35. J. Bai, R. Song, J. Fan, *et al.*, "Quantum defects of nF$_J$ levels of Cs Rydberg atoms," Phys. Rev. A **108**(2), 022804 (2023).
36. J. Bai, R. Song, Z. Li, *et al.*, "Microwave spectroscopy and Zeeman effect of cesium (n+2)D$_{5/2}$ →nF$_J$ Rydberg transitions," Phys. Rev. A **109**(2), 022818 (2024).
37. J. Fan, J. Bai, R. Song, *et al.*, "Microwave coupled Zeeman splitting spectroscopy of a cesium nP$_J$ Rydberg atom," Opt. Express **32**(6), 9297 (2024).
38. P. J. Mohr, B. N. Taylor, and D. B. Newell, "CODATA recommended values of the fundamental physical constants: 2006," J. Phys. Chem. Ref. Data **37**(3), 1187–1284 (2008).